Improvements in photostability and sensing properties of EuVO4 nanoparticles by microwave-assisted sol–gel route for detection of H2 O2 vapors

Chrystel Ambard, Natacha Duée, Franck Pereira, David Portehault, Christophe Méthivier, Claire-Marie Pradier, Clément Sanchez

Improvements in photostability and sensing properties of $EuVO_4$ nanoparticles by microwave assisted sol-gel route for detection of H_2O_2 vapors

Chrystel Ambard*[a], Natacha Duée, Franck Pereira[a,e], David Portehault[b], Christophe Méthivier[c,d,e], Claire-Marie Pradier[c,d,e], Clément Sanchez[b]

[a]CEA DAM Le Ripault F-37260, Monts, France

[b]Sorbonne Universités, UPMC Univ Paris 06, CNRS, Collège de France, Laboratoire de Chimie de la Matière Condensée de Paris (LCMCP), 11 place Marcellin Berthelot, F-75005, Paris, France

[c]Sorbonne Universités, UPMC Univ. Paris 06, Laboratoire de Réactivité de Surface, 4 place Jussieu, F-75005 Paris, Franceb

[d]CNRS, UMR 7197, Laboratoire de Réactivité de Surface, F-75005 Paris, France

[e]LRC CEA UPMC CNRS N°1

*Corresponding author: chrystel.ambard@cea.fr, Tel: +33(0)2 47 34 49 19, Fax: +33(0)2 47 34 51 83

Abstract

The inorganic thin-film fluorescence probe, with the advantages of long life span and high sensitivity, has attracted much attention in explosive detection. The poor ultraviolet absorption and lack of an aromatic ring make peroxide-based explosives very hard to detect. As the signature compound of peroxide-based explosives, H_2O_2 vapor detection became more and more important. Rare-earth doped vanadate is considered to be a suitable material for the detection of hydrogen peroxide due to the quenching of its fluorescence in the presence of hydrogen peroxide. Its only drawback lies on its poor photostability. In this work, we have developed a new synthesis to limit the photobleaching of $EuVO_4$-based films. We propose herein an original protocol using micro-wave assisted sol-gel route. The photostability of luminescent $EuVO_4$ has been achieved and the sensitivity has been greatly increased. The detection limit for H_2O_2 vapor is as low as 100 parts per billion (ppb). The characterization of these nanoparticles by photoelectron spectroscopy clearly correlates their sensitivity to H_2O_2 to the surface chemistry.

Keywords :
Rare-earth vanadate nanoparticles
Hydrogen peroxide detection
Anti-photobleaching
Microwave-assisted sol-gel route

1. Introduction

Sensing of hydrogen peroxide (H_2O_2) is of importance in several fields such as pharmaceutical, cosmetic [1], chemical industries [2] as well as biology [3, 4], environment [5] or food-processing [6]. H_2O_2 is also a precursor and a decomposition product of organic peroxides such as triactetone triperoxide (TATP) [7], involved in terrorist activities. Hence, detection and quantification of H_2O_2 is a major concern for safety applications.

Many workers in the past have reported detection of H_2O_2 vapors by employing mainly electrochemical methods using modified working electrodes [8-10] or amperometric detection [11]. Smart fluorescence quenching sensing methods have also been reported and are promising for rapid and sensitive detection of explosives [12]. Among them one of the most commonly used functional group is an aromatic boron ester or acid [13-15]. Their performances are closely linked to the sensitive materials used. Fluorescent organic materials are competitive in terms of sensitivity and response time but their lack of photostability and life span are major drawbacks. Sol-gel inorganic materials for sensitive coatings [16] present a much longer life span. However photostability remains a problem for continual use.

The $EuVO_4$ system has been already described elsewhere for different applications [17-20] especially for H_2O_2 detection in liquids [21-23]. The role of the synthesis route on detection performances was clearly demonstrated, in particular the choice of microwave (MW) for heat treatment [23]. For organic systems, the MAMEF effect (microwave accelerated metal-enhanced fluorescence) combining metal-enhanced fluorescence (MEF), that can dramatically increase the quantum yield and photostability of weakly fluorescing species, with the use of low-power MW, was successfully applied for immunoassays [24]. For inorganic systems, photo- and pH-stability of fluorescent silicon quantum dots (SiQDs) [25] were improved by one-pot microwave-assisted synthesis. An increase of the luminescence intensity of $EuVO_4$ NP obtained by microwave (MW) irradiation-assisted soft template synthesis were briefly described [26]. Nevertheless, these works were not dedicated to enhancement of detection performances such as photostability and quantum yield. Gaseous detection of H_2O_2 based on $EuVO_4$ sensors was also not presented before, to the best of our knowledge.

Herein we present improvements of the synthesis process leading to photostable films and efficient gaseous H_2O_2 sensors based on $EuVO_4$ nanoparticles. After conceiving a reliable H_2O_2 vapors generation system we have developed a new sol-gel route combining pH regulation over the whole precipitation process and a microwave heat treatment. The goal was to obtain a photostable and highly sensitive materials for H_2O_2 detection in gaseous phase. This paper describes a novel approach consisting in the synthesis of $EuVO_4$ nanoparticles, sensitive to H_2O_2 exposure, following two possible protocols. These nanoparticles were also characterized by photoelectron spectroscopy in order to correlate their sensitivity to H_2O_2 to the surface chemistry.

2. Materials and methods

2.1. Syntheses

All chemicals were purchased from Sigma Aldrich with synthesis reagent grade (>99% purity) and used without further purification.

The syntheses are detailed elsewhere [23]. Protocols are presented below.

The titrator used to ensure constant pH in methods **a** and **b** was a Titroline alpha Schott apparatus. The microwave oven was an Anton Paar Synthos 3000 multimode oven equipped with an immersion temperature probe. The temperature was raised to 150 °C in 3 min and maintained during 15 min.

*Method **a***. $EuVO_4$ nanoparticles were synthesized by precipitation. 50 mL of a solution of $Eu(NO_3)_3,5H_2O$ with a total concentration of metal cations 0.1 $mol \cdot L^{-1}$ was added dropwise to 37.5 mL of a 0.1 $mol \cdot L^{-1}$ Na_3VO_4

solution at pH 12.5. A white precipitate appeared. pH decreased during the addition. Once the pH reached 9, a titration device was used to maintain a constant pH value, by adding aliquots of a 0.2 mol·L^{-1} solution of tetramethylammonium hydroxide. After the addition was completed, the suspension was treated in a microwave oven during 15 min at 150 °C corresponding to an internal pressure of the reactor of 4.7 bar. After cooling, the suspension was dialyzed against water over three days, during which water was renewed two times a day. The molecular weight cut-off of the dialysis membrane was 3500 Da. Powders were collected by drying of the colloidal solutions at ambient temperature. In addition, the obtained opaque suspension can have been either diluted by water to a concentration of 10^{-3} mol·L^{-1}, or dialyzed a second time against ethanol for solvent exchange.

*Method **b***. The procedure was similar as method **a**, except that the thermal treatment under microwave irradiation was replaced by conventional heating at 60 °C for 30 min. Purification and powders recovery were performed as in method **a**.

*Method **c***. $EuVO_4$ nanoparticles were synthesized by precipitation according to a protocol proposed by Huignard et al.[27] using citrate ions to limit the growth of the nanoparticles and to stabilize the colloidal solution. Briefly, 30 mL of a 0.1 mol·L^{-1} solution of sodium citrate was added to 40 mL of a solution of $Eu(NO_3)_3$,$5H_2O$ with a total concentration of metal cations reaching 0.1 mol·L^{-1}. 30 mL of a 0.1 mol·L^{-1} Na_3VO_4 solution at pH 12.5 was then added to the mixture. The solution was aged during 30 min at 60 °C. Purification and powders recovery were performed as in method **a**.

2.2. Characterizations

Absorption spectra were recorded on a Lambda 900 Perkin Elmer spectrometer. Excitation and emission spectra, as well as photobleaching curves, were recorded on a Horiba Jobin Yvon Fluoromax-P spectrophotometer. Photobleaching curves were obtained by acquiring the evolution of the 617 nm emission intensity under a continuous excitation at 270 nm. The quantum yields were calculated using the following equation, valid for an optical density ranging between 0.01 and 0.1.

$$Q = Q_R \cdot \left(\frac{m}{m_R}\right) \cdot \left(\frac{n^2}{n_R^2}\right)$$

with *R* referring to the reference fluorophore (rhodamine 6G), *Q* the quantum yield, *m* the slope of the straight line (area of the fluorescence peak) = f (absorbance at 280 nm), *n* the refractive index of the solvent. Luminescence measurements were performed using an excitation wavelength of 280 nm at 21 °C.

XPS spectra were collected on a SPECS (Phoibos 100-1D Delay Line Detector) X-ray photoelectron spectrometer, using a monochromatized AlKα (1486.6 eV) X-ray source having a 300W (20 mA, 15 kV) electron beam power. Fixed Analyser transmission and a 7x20 mm entrance slit were used leading to a resolution of 0.1 eV for the spectrometer.The emissions of photoelectrons from the sample were analyzed at a takeoff angle of 90° under ultra-high vacuum conditions (1×10^{-8} Pa). High resolution spectra were collected at a pass energy of 20 eV for V and Eu core XPS levels.

Microstructural characterizations (TEM, XRD) and specific areas measurements of $EuVO_4$ nanoparticles were detailed and discussed previously [23].

2.3. Sample preparation for gaseous detection tests and XPS analysis

The solvent of the colloidal sol was modified through a dialysis step in ethanol described before. The substrates used were made of Suprasil quartz. The quartz surface preparation consisted in successive acetone cleaning, 10% wt. NaOH etching, washing with deionized water, optical soap, deionized water and then ethanol rinsing. Films of $EuVO_4$ nanoparticles were prepared from the alcoholic sol by a single step dip-coating. The sol concentration was 3% wt. The retrieval speed was 15 $cm.min^{-1}$. The temperature and the relative humidity of the room were regulated at 20±1°C/45±5% HR. Porous fragile films were obtained with a thickness around 100 nm.

2.4. H_2O_2 vapors generation system

The hydrogen peroxide vapors were produced by circulating an air flow into a thermostated cell containing liquid H_2O_2 (Figure 1). The vapors concentration can be modified by various ways: by a temperature variation of the cell, by bubbling the air into the $H_2O_{2(l)}$ container or by circulating it into the headspace, by a change of the $H_2O_{2(l)}$ concentration, by varying the rate of the air flow, etc. The dry and humid air lines were connected to produce air with a controlled humidity. The humidity level chosen for our experiments was 45 % and was the same as the humidity measured in the H_2O_2 vapor flow when generating a concentration of 1 ppm.

When generating low concentrations of H_2O_2 (typically less than 5 ppm), the PVC pipes retained partly the peroxide and a few minutes were required to obtain the good concentration in the spectrofluorometer. A saturation of the pipe was therefore performed before the detection tests, allowing to diffuse nearly instantly a known concentration of the gas.

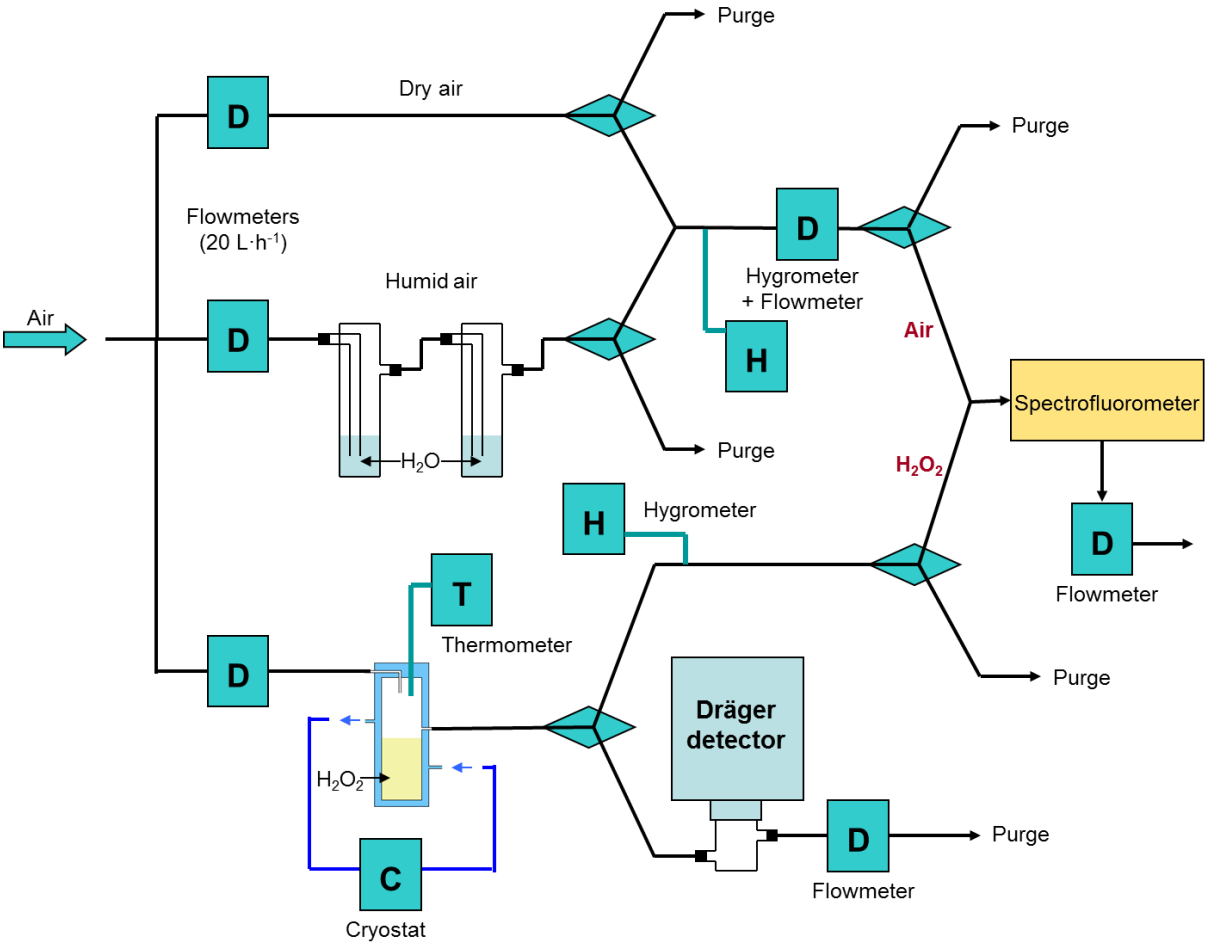

Figure 1. H_2O_2 vapors generation system

The detection was revealed by monitoring the fluorescence intensity before, during and after the exposure to the target gas. The measure was organized in three steps as shown in Figure 2.

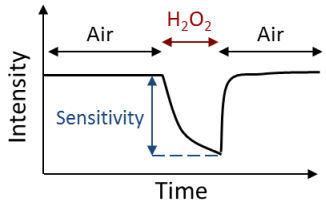

Figure 2**.** Detection test sequence

Firstly, the baseline was acquired during 30 minutes: the sensitive film was exposed to an air flow (with a controlled humidity). Then the film was exposed to vapors of H_2O_2 during 10 minutes. Finally, the sample was exposed to air flow again (with a controlled humidity) in order to evaluate the detection reversibility.

3. Results and discussion

3.1. Sensitivity and quantum yield

During the first step of the detection test, the baseline depends on the material. While it was constant with $EuVO_4$ prepared from method **a**, baselines for $EuVO_4$ from methods **b** and **c** showed an important decrease of the luminescence intensity due to the photobleaching of the nanoparticles (Figure 3). The MW treatment increased tremendously the photostability of $EuVO_4$. This point is detailed below in section 3.2. Whatever the synthesis route, subsequent exposure of the sensitive material to H_2O_2 vapors led to a rapid decrease of the fluorescence intensity. The amplitude of this extinction of fluorescence was clearly dependent on the synthesis conditions. The lowest sensitivity was achieved for method **c**, with a detection limit of about 1.5 ppm (Table 1). The presence of citrates at the surface of the particles may have restricted the interaction between H_2O_2 vapors and $EuVO_4$ material. The highest sensitivity was obtained with method **a**. Previous works have demonstrated the difference of microstructure induced by synthesis conditions [23]. In particular, the better crystallinity and lower defects concentration reached by efficient microwave heating associated seem to favor high sensitivity. During the last step of the test, the initial intensity was not recovered. The detection process was not reversible.

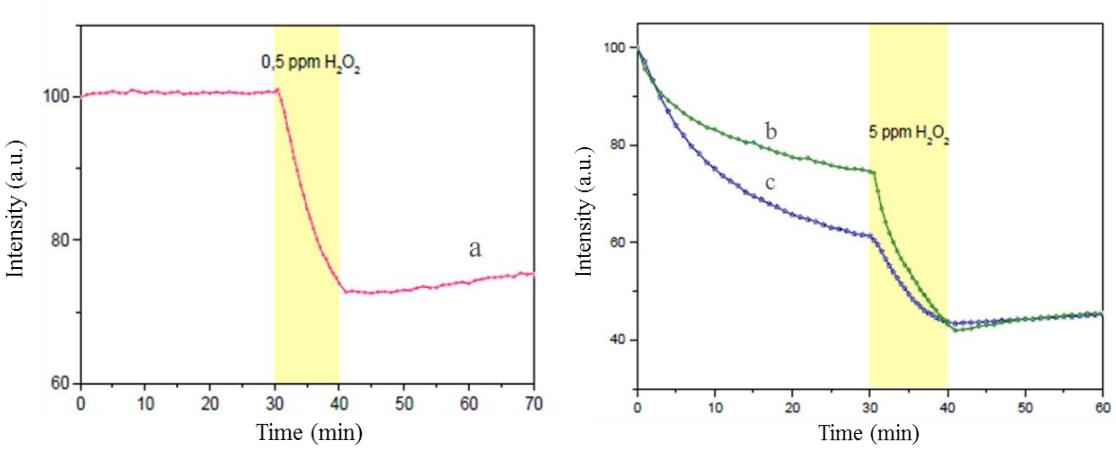

Figure 3. Detection tests of H_2O_2 vapors (λ_{exc} = 270 nm, λ_{em} = 617 nm) by $EuVO_4$ films prepared from methods **a**, **b** and **c**

Quantum yields (see Table 1) were slightly smaller than reported in the literature [28]. As explained before, this may have been related to the size of our particles (about 15 nm). Riwotzi et al. [29] reported that energy transfer to europium could only take place from vanadate first neighbors. Therefore, transfers from distant vanadate groups to surface sites are highly probable in nanoparticles, leading to de-excitation of the vanadate species. Consequently, quite low quantum yields were observed. As described in our previous works [23], the microwave treatment of method **a** improved efficiently the quantum yield compared to methods **b**. This phenomenon may have originated again from the better crystallinity yielded by efficient microwave heating that resulted in lower defect concentrations.

Table 1. Detection limits and quantum yields of $EuVO_4$ colloids

Sample	Preparation method	Detection limit of H_2O_2 vapors (ppm)	Quantum yield (%)

$EuVO_4$	a	0.1	7.8 ± 0.1
$EuVO_4$	b	0.6	3.0 ± 0.1
$EuVO_4$	c	1.5	5.5 ± 0.1

3.2. Photostability

The photostability is a key property for robust sensitive materials. When irradiating $EuVO_4$ films prepared from method **c** with UV, an important photobleaching phenomenon was observed (see Figure 4). A loss of about 80% of the fluorescence intensity at 617 nm followed by an asymptotic behavior after 10 consecutive UV irradiations occurred. Photobleaching in citrate-derived vanadates has also been reported previously [30]. Takeshita et al. showed that surface-complexing citrate anions are involved in the photobleaching process.

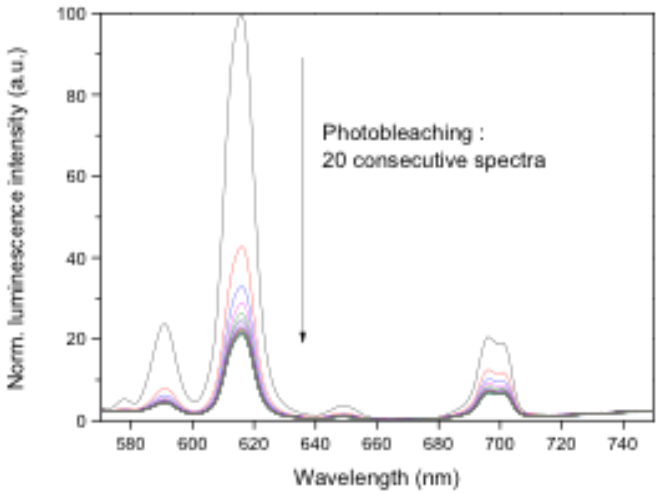

Figure 4. Emission spectrum evolution under UV irradiation (λ_{exc} = 270 nm) of $EuVO_4$ films prepared from method **c**: photobleaching induced by 20 consecutive acquisitions

Photobleaching of $EuVO_4$ films prepared from methods **a**, **b** and **c** was very fast under UV irradiation (Figure 5). The decrease in the luminescence intensity was higher for method **c** than for methods **a** or **b** due to the presence of citrate ions on the particles. When eliminating citrates, the photostability strongly increased. Photobleaching was negligible for method **a**. These results showed that the structure and the surface state were also involved in photobleaching. MW heat treatment allowed producing a photostable sensitive material. Consequently, the lifespan of the material during the use of the sensor might have been extended.

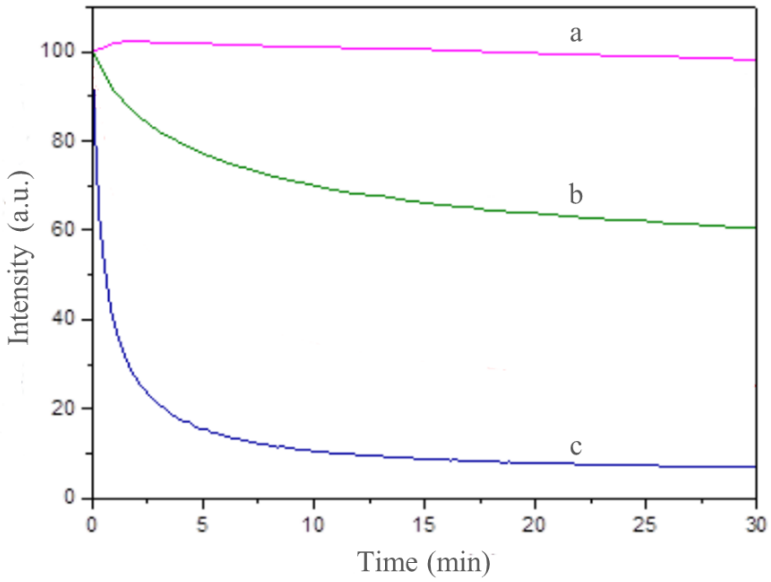

Figure 5. Photobleaching curves (l_{exc}=270 nm, l_{em}=617 nm) of $EuVO_4$ films prepared from **methods a**, **b** and **c**

3.3. XPS analysis

A particular interest was dedicated to particles surfaces because of their unique role in the interaction, and thus detection of vapors by nanoparticles. XPS analysis was achieved in order to make clear potential modifications of the surface induced by H_2O_2 exposure. XPS analysis indicated the presence of hydroxyl- groups, V^{5+}, V^{4+}, Eu^{3+} and Eu^{2+} on the surface of the particles, prepared following protocol **b**, before exposure to the target gas (see Figure 6 and Figure 7); note that adsorbed water molecules were detected, in addition to all other compounds, after synthesis following protocol **a**. Apart from this point, very similar surfaces compositions were observed for sensitive materials obtained from methods **a** and **b**. The effect of the hydrogen peroxide on the Eu^{2+}/Eu^{3+} ratio was significant, as Eu^{2+} disappears and Eu became fully oxidized under exposure to oxidizing H_2O_2. The presence of V^{4+} may have been induced by photoemission itself and could have explained why the concentration of V^{4+} remained almost constant. After exposure to H_2O_2 vapors, the relative amount of –OH groups on the surface was increased. In addition, the sample prepared according to protocol **a** (Figure 7) also exhibited a large amount of adsorbed water after exposure to H_2O_2. OH groups were known to reduce the quantum yield of fluorescence of nanoparticles. Hence, the observed surface modifications may have explained fluorescence quenching observed during peroxide exposure [31].

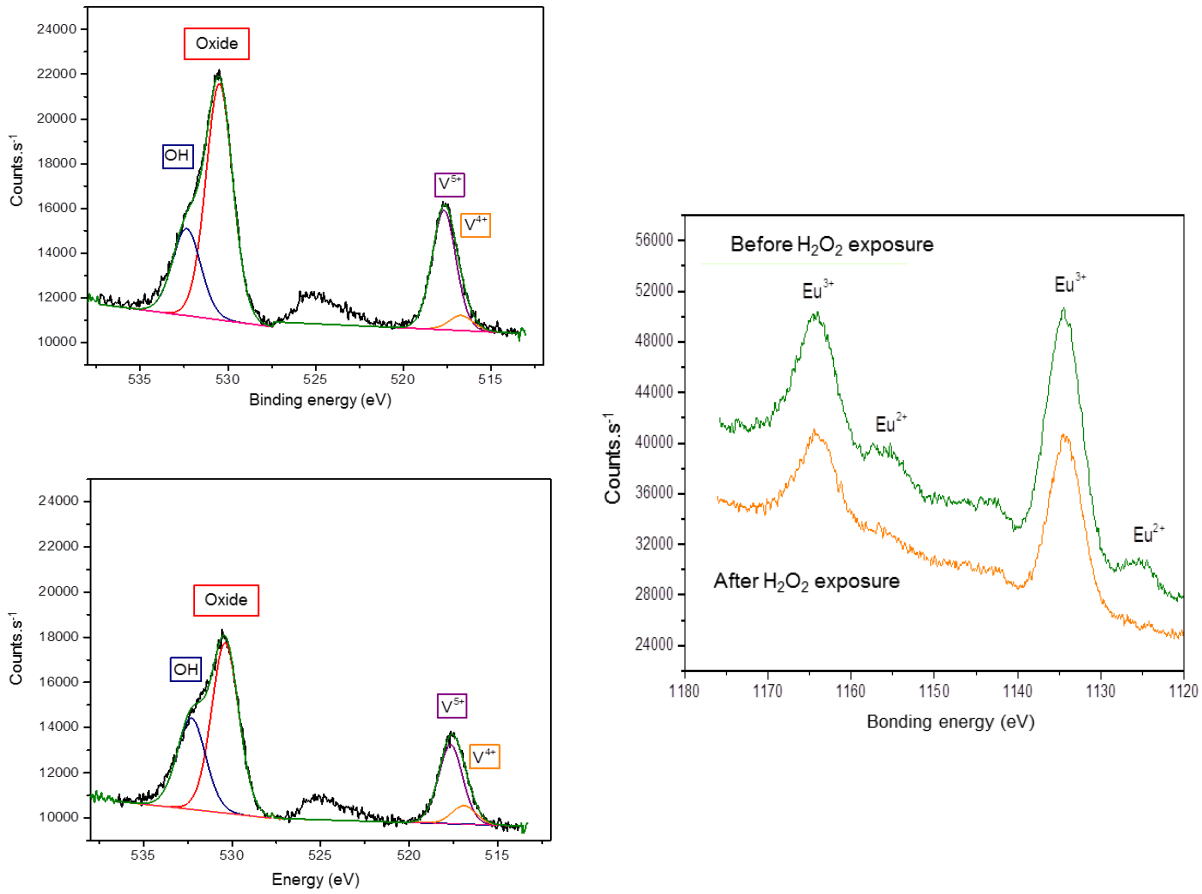

Figure 6. XPS of $EuVO_4$ nanoparticles prepared from method **b**:
top left: before H_2O_2 exposure, bottom left : after H_2O_2 exposure

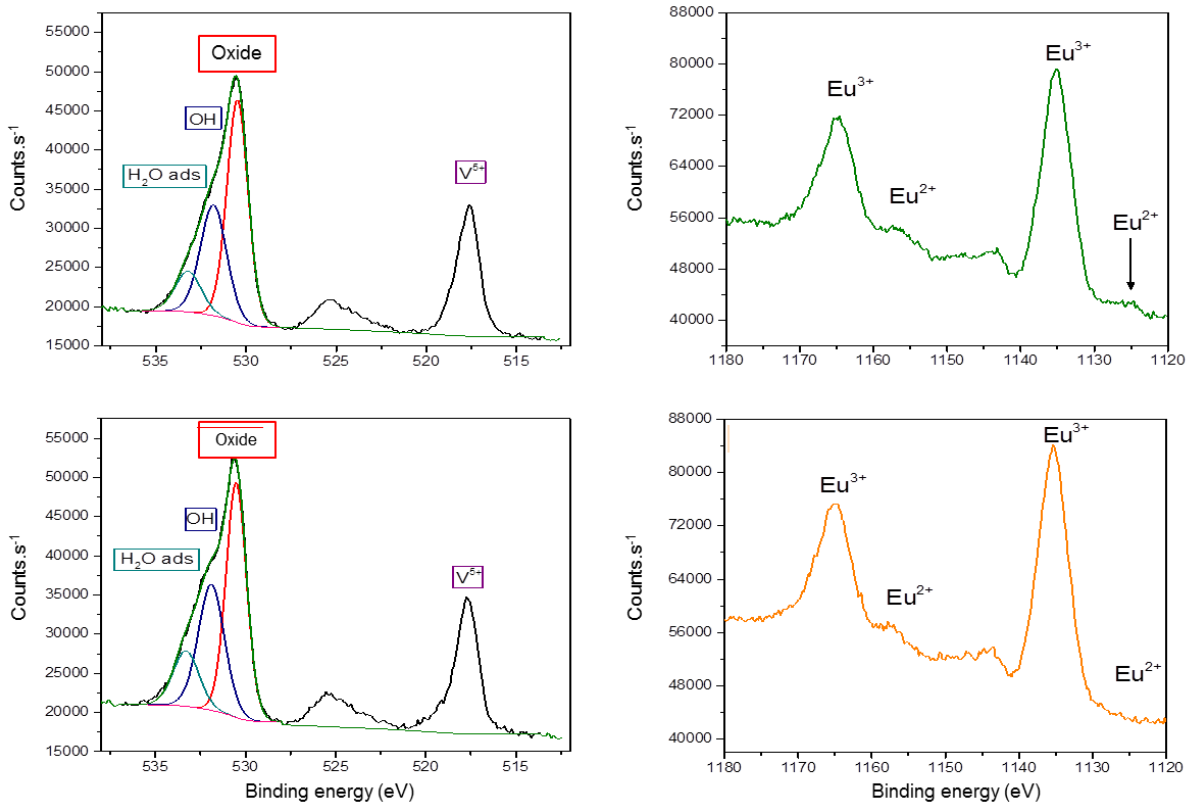

Figure 7. XPS spectra of $EuVO_4$ nanoparticles prepared from method **a**:
top : before H_2O_2 exposure, bottom : after H_2O_2 exposure

To compare the synthesis methods and interpret the quenching phenomena, the ratio of hydroxyl- groups plus water molecules, over the contribution of oxygen in the oxides, was calculated by integrating the XPS contributions. Results reported in Table 2 show a lower concentration of –OH groups (and H_2O) for materials obtained from method **a** than from method **b**. These groups decrease the probability of a radiative transition. This may consequently have explained the decrease of the quantum yield previously observed.

Table 2. Relative concentrations of surface hydroxyl- groups and water molecules on the surface of $EuVO_4$ nanoparticles estimated by XPS

Material	$\frac{[H_2O_{ads} + OH^-]}{[O^{2-}]}$	
	Before H_2O_2 vapors exposure	After H_2O_2 vapors exposure
$EuVO_4$ method **a**	0.84	0.98
$EuVO_4$ method **b**	1.00	1.14

4. Conclusions

This work confirms the impact of soft chemistry synthesis conditions on the performances of optical hydrogen peroxide sensors. We have developed a very photostable and sensitive material for gaseous detection of H_2O_2 about a hundred of ppb. These results have been patented [32]. Further studies are underway to ascertain the exact detection mechanism. Besides, as these soft chemistry-derived materials compare favorably to state-of-art inorganic and organic optical materials in terms of stability and sensitivity, we are currently performing field tests by implementing the fluorescent sensor in a portable device, suitable for operation in public places. This work will be published elsewhere.

Acknowledgments

References

1. Campanella L, Roversi R, Sammartino MP, Tomassetti M (1998) Hydrogen peroxide determination in pharmaceutical formulations and cosmetics using a new catalase biosensor. J Pharmaceut Biomed 18:105-116
2. Usui Y, Sato K, Tanaka M (2003) Catalytic dihydroxylation of olefins with hydrogen peroxide: An organic-solvent- and metal-free system. Angew Chem Int Edit 42:5623-5625
3. Niethammer P, Grabher C, Look AT, Mitchison TJ (2009) A tissue-scale gradient of hydrogen peroxide mediates rapid wound detection in zebrafish. Nature 459:996-999
4. Wang T, Zhu H, Zhuo J, Zhu Z, Papakonstantinou P, Lubarsky G, Lin J, Li M (2013) Biosensor based on ultrasmall MoS_2 nanoparticles for electrochemical detection of H_2O_2 released by cells at the nanomolar level. Anal Chem 85:10289-10295
5. Wang Y, Huang J, Zhang C, Wei J, Zhou X (1998) Determination of hydrogen peroxide in rainwater by using a polyaniline film and platinum particles co-modified carbon fiber microelectrode. Electroanal 10:776-778
6. Kirchner P, Li B, Spelthahn H, Henkel H, Schneider A, Friedrich P, Kolstad J, Keusgen M, Schoning MJ (2011) Thin-film calorimetric H_2O_2 gas sensor for the validation of germicidal effectivity in aseptic filling processes. Sensor Actuat B- Chem 154:257-263
7. Mahbub P, Wilson R, Nesterenko PN (2016) Ultra-fast continuous-flow photo degradation of organic peroxide explosives for their efficient conversion into hydrogen peroxide and possible application. Propell Explos Pyrot
8. Shaojun Y, Shuai Y, Junhui X, Ying W, Jianlin L, Shengshui H (2006) A hydrogen peroxide sensor based on colloidal MnO_2/Na-montmorillonite. Appl Clay Sci 33:35-42
9. Reisert S, Schneider B, Geissler H, van Gompel M, Wagner P, Schoning MJ (2013) Multi-sensor chip for the investigation of different types of metal oxides for the detection of H_2O_2 in the ppm range. Phys Status Solidi A 210:898-904
10. Hennemann J, Kohl CD, Reisert S, Kirchner P, Schoning MJ (2013) Copper oxide nanofibres for detection of hydrogen peroxide vapour at high concentrations. Phys Status Solidi A 210:859-863
11. Wiedemair J, van Dorp HDS, Olthuis W, van den Berg A (2012) Developing an amperometric hydrogen peroxide sensor for an exhaled breath analysis system. Electrophoresis 33:3181-3186
12. McQuade DT, Pullen AE, Swager TM (2000) Conjugated polymer-based chemical sensors. Chem Rev 100:2537-2574
13. Fu Y, Yao J, Xu W, Fan T, Jiao Z, He Q, Zhu D, Cao H, Cheng J (2016) Schiff base substituent-triggered efficient deboration reaction and its application in highly sensitive hydrogen peroxide vapor detection. Anal Chem
14. Bohrer FI, Colesniuc CN, Park J, Schuller IK, Kummel AC, Trogler WC (2008) Selective detection of vapor phase hydrogen peroxide with phthalocyanine chemiresistors. J Am Chem Soc 130:3712
15. Verma AL, Saxena S, Saini GSS, Gaur V, Jain VK (2011) Hydrogen peroxide vapor sensor using metal-phthalocyanine functionalized carbon nanotubes. Thin Solid Films 519:8144-8148
16. Lukowiak A, Strek W (2009) Sensing abilities of materials prepared by sol–gel technology. Journal of Sol-Gel Science and Technology 50:201-215
17. Riwotzki K, Haase M (1998) Wet-chemical synthesis of doped colloidal nanoparticles: YVO_4 : Ln (Ln = Eu, Sm, Dy). J Phys Chem B 102:10129-10135

18. Pan G, Song H, Bai X, Liu Z, Yu H, Di W, Li S, Fan L, Ren X, Lu S (2006) Novel energy-transfer route and enhanced luminescent properties in $YVO_4:Eu^{3+}/YBO_3:Eu^{3+}$ composite. Chem Mater 18:4526-4532
19. Hou ZY, Yang PP, Li CX, Wang LL, Lian HZ, Quan ZW, Lin J (2008) Preparation and luminescence properties of YVO_4:Ln and $Y(V,P)O^{-4}$:Ln (Ln = Eu^{3+}, Sm^{3+}, Dy^{3+}) nanofibers and microbelts by sol-gel/electrospinning process. Chem Mater 20:6686-6696
20. Wu CC, Chen KB, Lee CS, Chen TM, Cheng BM (2007) Synthesis and VUV photoluminescence characterization of $(Y,Gd)(V,P)O^{-4}$: Eu^{3+} as a potential red-emitting PDP phosphor. Chem Mater 19:3278-3285
21. Abdesselem M, Schoeffel M, Maurin I, Ramodiharilafy R, Autret G, Clément O, Tharaux P-L, Boilot J-P, Gacoin T, Bouzigues C, Alexandrou A (2014) Multifunctional rare-earth vanadate nanoparticles: Luminescent labels, oxidant sensors, and MRI contrast agents. ACS Nano 8:11126-11137
22. Casanova D, Bouzigues C, Nguyen T-L, Ramodiharilafy RO, Bouzhir-Sima L, Gacoin T, Boilot J-P, Tharaux P-L, Alexandrou A (2009) Single europium-doped nanoparticles measure temporal pattern of reactive oxygen species production inside cells. Nat Nanotechnol 4:581-585
23. Duée N, Ambard C, Pereira F, Portehault D, Viana B, Vallé K, Autissier D, Sanchez C (2015) New synthesis strategies for luminescent YVO_4: Eu and $EuVO_4$ nanoparticles with H_2O_2 selective sensing properties. Chem Mater 27:5198-5205
24. Aslan K, Geddes CD (2005) Microwave-accelerated metal-enhanced fluorescence: Platform technology for ultrafast and ultrabright assays. Anal Chem 77:8057-8067
25. He Y, Zhong Y, Peng F, Wei X, Su Y, Lu Y, Su S, Gu W, Liao L, Lee S-T (2011) One-pot microwave synthesis of water-dispersible, ultraphoto- and pH-stable, and highly fluorescent silicon quantum dots. J Am Chem Soc 133:14192
26. Huong TT, Tu VD, Anh TK, Vinh LT, Minh LQ (2011) Fabrication and characterization of $YVO_4:Eu^{3+}$ nanomaterials by the microwavetechnique. J Rare Earth 29:1137
27. Huignard A, Gacoin T, Boilot J-P (2000) Synthesis and luminescence properties of colloidal YVO_4:Eu phosphors. Chem Mater 12:1090-1094
28. Huignard A, Buissette V, Franville AC, Gacoin T, Boilot J-P (2003) Emission processes in YVO_4:Eu nanoparticles. J Phys Chem B 107:6754-6759
29. Riwotzki K, Haase M (2001) Colloidal YVO_4:Eu and $YP_{0.95}V_{0.05}O_4$: Eu nanoparticles: Luminescence and energy transfer processes. J Phys Chem B 105:12709-12713
30. Takeshita S, Ogata H, Isobe T, Sawayama T, Niikura S (2010) Effects of citrate additive on transparency and photostability properties of $YVO_4:Bi^{3+},Eu^{3+}$ nanophosphor. J Electrochem Soc 157:J74-J80
31. Buissette V, Giaume D, Gacoin T, Boilot JP (2006) Aqueous routes to lanthanide-doped oxide nanophosphors. Journal of Materials Chemistry 16:529-539
32. Ambard C, Duée N, Vallé K, Portehault D, Sanchez C (2014) Procédé de préparation d'une solution colloïdale de nanoparticules d'un oxyde de vanadium. French Patent N°14 61067